Available online at www.sciencedirect.com
ScienceDirect
Journal of Power Sources 172 (2007) 379–387
JOURNAL OF POWER SOURCES
www.elsevier.com/locate/jpowsour

$CoFe_2O_4$ and $NiFe_2O_4$ synthesized by sol–gel procedures for their use as anode materials for Li ion batteries

P. Lavela*, J.L. Tirado

Laboratorio de Química Inorgánica, Universidad de Córdoba, Campus de Rabanales, 14071 Córdoba, Spain

Received 15 March 2007; received in revised form 28 June 2007; accepted 29 July 2007
Available online 3 August 2007

Abstract

Cobalt and nickel spinel ferrites with $CoFe_2O_4$ and $NiFe_2O_4$ stoichiometries have been prepared by a sol–gel process based on a vacuum sublimation of a citrate precursor. Several samples of $CoFe_2O_4$ were obtained by varying the conditions of citrate precursor formation and further annealing. SEM images demonstrated the strong influence of synthesis parameters on the morphologies of secondary and primary particles. The formation of layered flake-like aggregates defining a macroporous system is assumed to improve the electrolyte–electrode contact in iron-containing samples. An enhanced electrochemical performance was achieved for samples annealed at high temperatures, especially for $CoFe_2O_4$ heated at 1000 °C for 24 h. Capacity values higher than 700 mAh g^{-1} was recorded after 75 cycles. ^{57}Fe Mössbauer spectroscopy was used to clarify aspects of the mechanism of the electrochemical reaction.

Keywords: Lithium; Batteries; Sol–gel; Citrate; Freeze-drying; Ferrite

1. Introduction

Conversion reactions have opened a new line of research in the field of electrode materials for Li ion batteries [1]. Transition metal oxides can be reduced to their metal state and then be reoxidized providing a large reversible capacity for a large number of cycles. Surprisingly, insertion and/or Li alloying reactions are not the main processes involved upon charge or discharge. Instead, a complete structural degradation occurring during the first discharge yields nano-sized particles of metal and Li_2O. Unlike to tin compounds, this alkaline oxide matrix is reversibly reduced on charging, reforming metal oxide and lithium [2,3]. Li_2O, intimate mixed with metallic particles may act as an oxygen reservoir promoting metal oxidation [4]. Conversion reactions have been also demonstrated for other compounds as nitrides, halides, sulfides [5–7], etc. In most cases, the reversibility of the lithium salt has been evidenced as responsible of the cell cycling [8], but for Cu_3N, the oxidation of Cu to form CuO contributes to the increase of capacity with cycle number [9].

Another interesting feature concerning this kind of lithium reaction involves the formation of an organic polymeric layer wrapping the discharged products. Some authors have proposed the presence of oligomer chains of poly(ethylene oxide) produced from solvent decomposition and CO_2 release [10]. This layer is continuously formed and dissolved on cycling not hindering the lithium migration from the electrolyte to the active material.

In previous works, our group has proposed the study of mixed transition metal oxides as $NiFe_2O_4$ and $NiCo_2O_4$ [11,12]. The use of Mössbauer and X-ray photoelectron spectroscopies allowed clarifying interesting features related to the reversible reaction with lithium and sodium. Nevertheless, the use of solid-state reaction or co-precipitation methods precluded the achievements of good electrochemical performances in a long-term cycling. Also, the influence of particle size effect has been reported [13,14] what lead us to search for alternative preparation routes. Because of the great success of these spinel type ferrites in the field of magnetic materials, a number of papers focused on the synthesis of nano-powdered particles are available [15–17]. Moreover, sol–gel methods have been successfully essayed on related oxides acting as electrodes in lithium cells [18]. Vacuum sublimation using a freeze dryer has been reported as a useful method to precipitate a citrate precursor with a ran-

* Corresponding author. Tel.: +34 957 218 637; fax: +34 957 218 621.
E-mail address: iq1lacap@uco.es (P. Lavela).

0378-7753/$ – see front matter © 2007 Elsevier B.V. All rights reserved.
doi:10.1016/j.jpowsour.2007.07.055

dom distribution of metals. Namely, finely disperse $LiCoO_2$ and $LiNiO_2$ were prepared [19,20].

The aim of this work is to test the influence of synthesis parameters as ligand to metal ratio, pH of the final solution and annealing conditions on particle morphology. Also, the evaluation of the electrochemical performance of lithium cells assembled with these materials, as working electrodes will be discussed.

2. Experimental

Spinel oxides with nominal stoichiometries $CoFe_2O_4$ and $NiFe_2O_4$ were prepared by a sol–gel method using a citrate ligand to complex the metal ions. For this purpose, a 0.3 M solution of both metals was prepared from the appropriated ratio of nitrate salts. Then citric acid was added to provide a 1:1 metal:citrate ratio, with a slight excess of 10% of the acid to ensure the complete chelation of the metal ions. The acidic solution was neutralized with 30% ammonium solution up to pH 7. The metal citrate solutions were freezed at −80 °C and then sublimated in a FTS System at −48 °C under 150 mT pressure for 48 h. The so obtained citrate precursor was collected, ground and stored in a MBraun glove box to preserve it from hydration. Alternatively, 1:2 metal:citrate ratio, more basic conditions (pH 10) or more diluted solution (0.15 M) were also tested for the preparation of $CoFe_2O_4$ precursor, named as $CoFe_2O_4$Cit2 and $CoFe_2O_4$pH10, $CoFe_2O_4$dil, respectively. $CoFe_2O_4$ precursor was annealed at several temperatures ranging from 600 to 1000 °C for 24 h in air atmosphere.

X-ray diffraction patterns were recorded in a Siemens D5000 Diffractometer, with a Cu Kα radiation (1.5406 Å) and a graphite monochromator. A scan velocity of $2°(2\theta)\,min^{-1}$ was set. The Service of Support to Research at the University of Córdoba provided a JEOL-SM6300 microscope to obtain SEM images of the annealed products. A FT-MIR Nicolet Magna-IR550 Series II spectrometer, with a $4\,cm^{-1}$ resolution in the spectral range covering 4000–400 cm^{-1}, was used.

^{57}Fe Mössbauer spectra (MS) experiments were recorded with an EG and G constant accelerator spectrometer in transmission mode and at room temperature. The source was ^{57}Co in a Rh matrix (10 mCi). The velocity scale was calibrated from the magnetic sextet of a high purity iron foil absorber. Experimental data were fitted to Lorentzian lines by using a least square based method [Landry F, Schaaf P. WinISO–Windows Mössbauer Fitting Programme (unpublished, 1998)]. The quality of the fit was controlled by the classical test of χ^2. All the isomer shifts are given relative to the center of the α-Fe spectrum at room temperature.

The electrochemical experiments were carried out by using two- and three-electrodes Swagelok type lithium cells. Counter and reference electrodes were 9 mm discs of lithium metal and the working electrode consisted of a mixture of 75% of active material and 10% of graphite, 10% of carbon black and 5% of PVDF binder were coated on a cooper foil of the same diameter. A 1 M $LiPF_6$ (EC:DEC = 1:1) electrolyte solution was supported in Whatman glass fiber discs. An Arbin potentiostat/galvanostat multichannel system was used to cycle two electrodes lithium cell at 1 C rate for both charge and discharge branches. Electrochemical impedance spectroscopy (EIS) was carried out in an Autolab PGSTAT12 system. A three-electrode lithium cell was successively cycled by passing current between the working electrode (evaluating material) and the counter electrode (Li). After a period of relaxation, at least 5 h, to achieve a quasi-equilibrium system, the impedance spectra were recorded versus a Li reference electrode. An ac voltage signal of 5 mV was applied from 100 to 2 mHz.

3. Results and discussion

The X-ray diffraction patterns of the precursors show a set of reflections indexed to ammonium nitrate arising from the used reagents, but no discernible peaks were observed which could be associated to the citrate salts. In fact, the presence of crystalline NH_4NO_3 has been also reported in similar procedures when pH values higher than four were fixed for the precursor solution [21]. In order to get a better characterization of the citrate precursor, FT-IR spectra were recorded. The spectrum for citric acid was included as a reference. The citric acid spectrum contains bands at 1760 and 1722 cm^{-1} ($\nu_{C=O}$); 1430 cm^{-1} (δ_{OH}(in-plane)), 1300–1200 cm^{-1} ($\nu_{C=O}$) and 930 cm^{-1}(δ_{OH}(out-of-plane)) revealing the presence of carboxylic groups. On increasing the metal:citric acid ratio used to obtained the precursor, we observe as these bands are progressively substituted by a new assembly of signals associated to deprotonated citrate groups. Thus, for the M:Cit 1:1 precursors, two characteristic vibrations of $-CO_2^-$, corresponding to the antisymmetric and symmetric stretching vibrations (ν_{as} and ν_s) located near 1630 and 1387 cm^{-1}, respectively, are predominant (Fig. 1).

Also, significant differences are observed in the spectrum region for which stretching vibrations of OH are visible. Thus, the narrow bands at 3500 and 3458 cm^{-1} and the broad bands at 3307 and 3230 cm^{-1}, revealing the occurrence of hydrogen bonding in the citric acid are substituted by one diffuse band at near 3158 cm^{-1} in the citrate salts corresponding to a protonated hydroxyl group. The broad band at about 3500 cm^{-1} can be attributed to crystallisation and/or coordination water. From

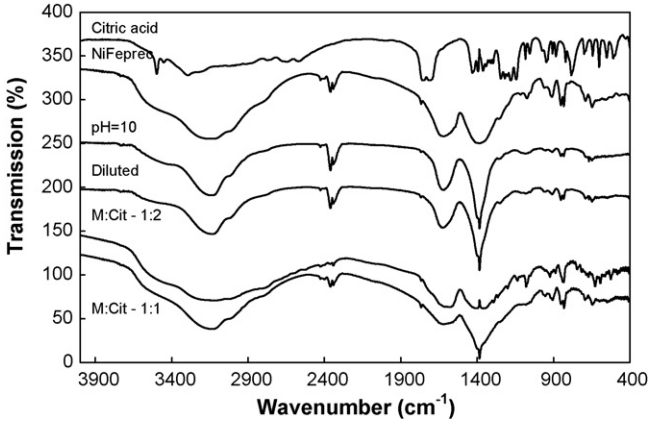

Fig. 1. FTIR spectra of citric acid and precursor citrates in the 4000–400 cm^{-1} range.

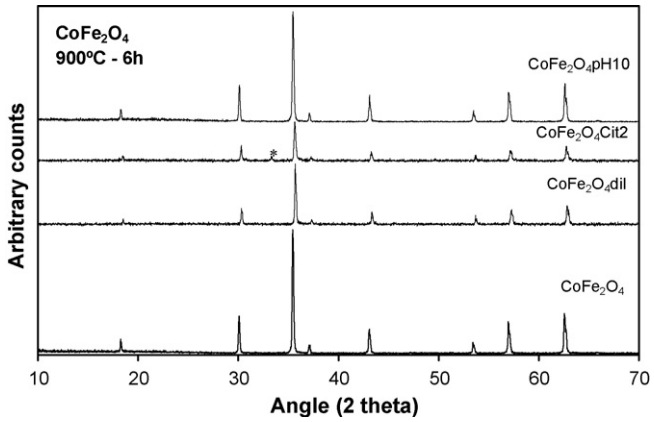

Fig. 2. XRD patterns of $CoFe_2O_4$ samples annealed at 900 °C for 6 h.

these results, a triionized citrate ligand chelating the transition metal ions can be inferred, though the presence of NH_4 groups (about 1460 cm^{-1}) may also contribute to the complex structure of the symmetric mode [20].

The XRD patterns of $CoFe_2O_4$ oxides obtained from different precursors and annealed at 900 °C for 6 h are depicted in Fig. 2. Narrow reflections ascribable to high crystalline $CoFe_2O_4$ are observed in all cases. An additional signal at ca. 33° (marked with an asterisk), for $CoFe_2O_4$Cit2, could be indicative of the presence of minor impurities, most probably due to hematite. Fig. 3 shows the SEM images corresponding to this set of $CoFe_2O_4$ samples. The preparation procedure of the precursor demonstrated to have a significant influence on the morphologies of the oxides. On increasing the amount of citric acid to a 1:2 M:Cit ratio (Fig. 3a), bulky particles constituted by the aggregation of 100–200 nm $CoFe_2O_4$ primary particles were grown. These particles are deposited in such way that big-circled pores (1–2 μm in diameter) are visible on the surface. The increase of the pH of the final solution to 10 (Fig. 3b), layered aggregates of submicronic primary particles appears now extremely corrugated forming an interleaved web of microfibers. Some authors have reported that the use of diluted solution favours the formation of smaller particles [22]. Bearing in mind this hypothesis, a 0.15 M metal solution was also prepared and freeze-dried (Fig. 3c). Unfortunately, our sample morphology showed a high coalescence of primary particles, forming less layered and porous particles.

The first galvanostatic cycles of lithium cells assembled with these oxides are plotted in Fig. 4. The first branch evidences an initial abrupt decrease of the cell potential followed by a steady plateau whose charge value agrees well with the electrons needed for the transition metal reduction to their metallic state according the following reaction:

$$CoFe_2O_4 + 8Li \rightarrow Co + 2Fe + 4Li_2O$$

in close relation with the mechanism reported for $NiFe_2O_4$ [11].

Some authors have reported the presence of several plateaus during the first discharge, which were ascribed to the sequential reduction of cobalt and iron, respectively, according to the length of the plateaus [23]. Also, lithium insertion in nano-sized hematite samples [14] and atoms ordering during CuO reduction were pointed out as responsible of the appearance of new plateaus at the beginning of the first discharge [4]. An structural degradation is also observed. At the end of the discharge, the cell voltage decreases more steeply to finally reach the lower cut off voltage at 0 V. In this last process, the electrons are consumed to built an organic polymeric layer coating the inorganic parti-

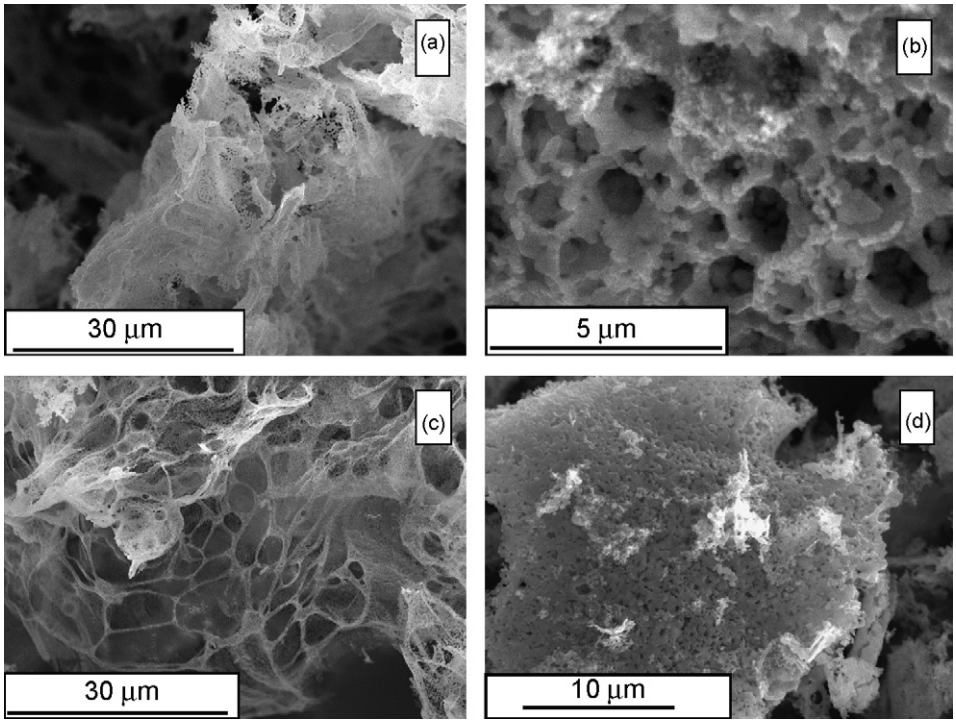

Fig. 3. SEM micrographs of $CoFe_2O_4$ samples: (a) $CoFe_2O_4$; (b) $CoFe_2O_4$Cit2; (c) $CoFe_2O_4$pH10; (d) $CoFe_2O_4$dil.

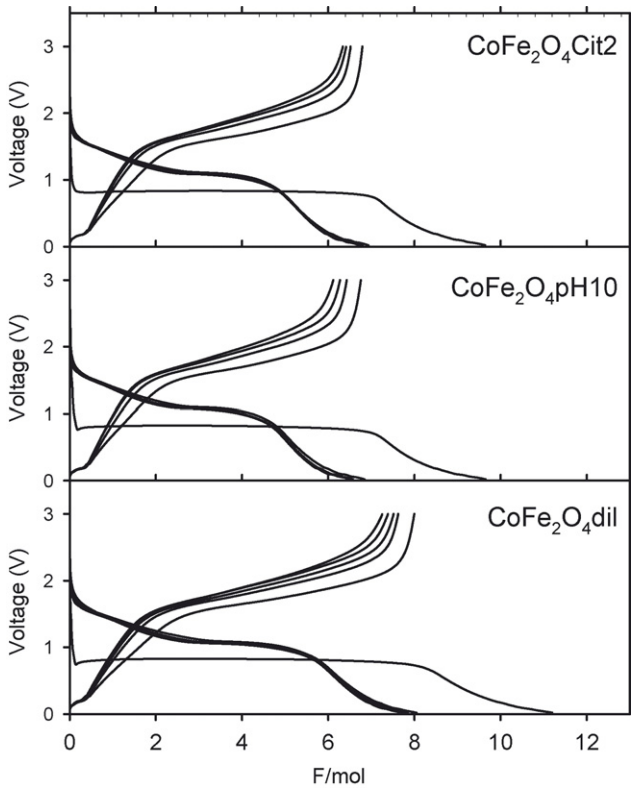

Fig. 4. Galvanostatic curves for the first three cycles for (a) $CoFe_2O_4$Cit2; (b) $CoFe_2O_4$pH10; (c) $CoFe_2O_4$dil. Cells were cycled at 1 C rate.

cles formed by the reduction. On charging, both the organic film and the reduction products are oxidised, although the retrieve of the crystalline structure is precluded. Because of the energetically distinct environments of metal atoms at the end of the first cycle, the second discharge shows a different profile in which the plateau has been substituted by a continuous decrease of voltage.

The extended galvanostatic cycling of these samples is shown in Fig. 5. The increase of pH to 10 did involve a loss of capacity

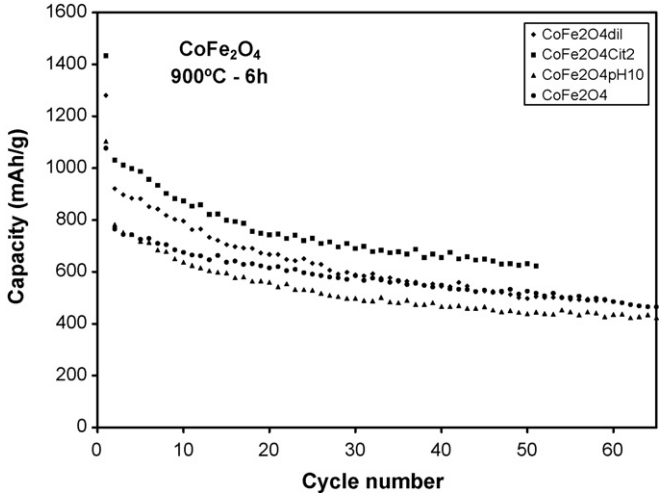

Fig. 5. Extended galvanostatic cycling of $CoFe_2O_4$, $CoFe_2O_4$Cit2, $CoFe_2O_4$pH10 and $CoFe_2O_4$dil annealed at 900 °C for 6 h. Cells were cycled at 1 C rate.

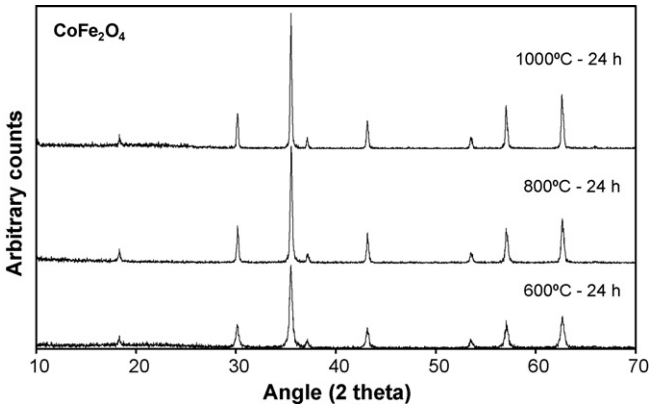

Fig. 6. XRD patterns of $CoFe_2O_4$ annealed at 600, 800 and 1000 °C for 24 h.

for the whole range of measured cycles. Probably the growth of the microfibers leads to a notorious decrease of sample surface hindering the lithium reaction. Higher capacity values were recorded for the lithium cell assembled with the $CoFe_2O_4$ sample obtained from a diluted solution. Nevertheless, the capacity fading was significant in a long-term cycling. The best capacity retention was monitored for samples prepared at pH 7 and 0.3 M in metal concentration. For a further optimization of the synthesis conditions, that precursor obtained with M:Cit 1:1 ratio was selected to prepare samples at different annealing temperatures.

The XRD patterns were always ascribable to pure and highly crystalline $CoFe_2O_4$ phases (Fig. 6). The broadening of the maxima decreased with temperature as expected from the sintering of particles. This fact could be more easily observed from the SEM images in Fig. 7. At the lowest temperature, the SEM images show that bulky aggregates of rough surface are developed. On increasing the annealing temperature, more layered particles are detected in which the macroporosity is still undeveloped. In turn, the precursor treated at 1000 °C for 24 h led to the formation of layered aggregates closely similar at those developed for iron samples heated at 900 °C. BET surface areas were 8.6 $m^2\,g^{-1}$ for the samples annealed at 600 °C, 4.7 $m^2\,g^{-1}$ for the 800 °C sample and 1.1 $m^2\,g^{-1}$ for that calcined at 1000 °C. Similar values have been reported for samples obtained by a thermal decomposition of an organic salt [20,24]. The electrochemical curves did not show remarkable variations arising from the changes in the synthesis parameter. In turn, the extended galvanostatic cycling evidenced significant differences in capacity fading (Fig. 8). The first evidence of the influence of the new annealing conditions on the electrochemical behaviour is a significant increase in the first discharge capacity and also a moderate decrease of the irreversibility in the first cycle when annealing time increased from 6 to 24 h. Nevertheless, the samples annealed at low temperatures were not able to retain cell capacity on extended cycling. On the contrary, the sample heated at 1000 °C provided capacity values as high as 740 mAh g^{-1} after 75 cycles. Again, we can explain the different electrochemical behaviour in terms of the morphological properties of the samples. Thus, the lack of a macroporosity and uncompleted crystallisation detected for samples obtained at 600 °C may be

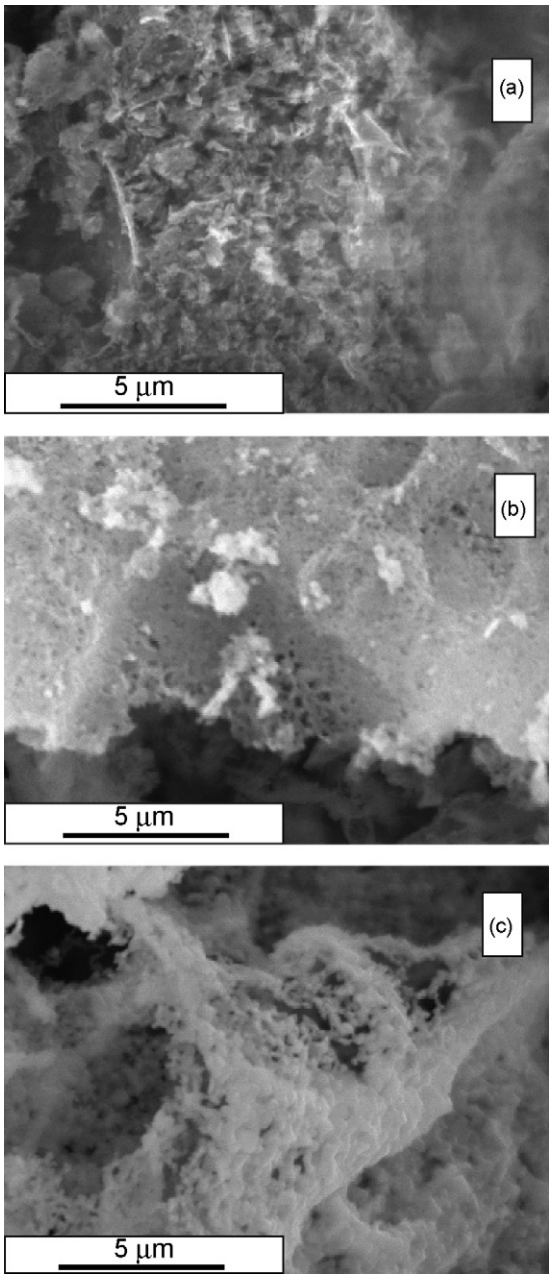

Fig. 7. SEM micrographs of $CoFe_2O_4$ samples annealed at (a) 600 °C, (b) 800 °C and (c) 1000 °C for 24 h.

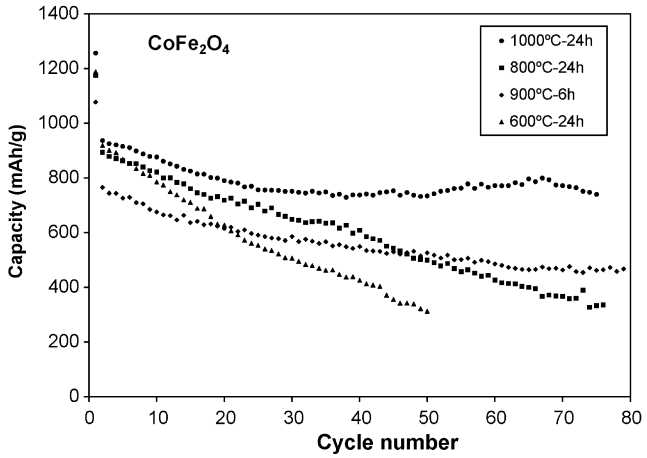

Fig. 8. Galvanostatic cycling of $CoFe_2O_4$ samples annealed at several temperatures. Kinetic rate: 1 C.

responsible of the poor performance. The development of the macroporous layered particles constituted by well-crystallised primary particles undoubtedly contributes to the improvement of the electrochemical behaviour. $CoFe_2O_4$ prepared as a polycrystalline material deposited in thin film was able to sustain about 610 mAh g^{-1} after 20 cycles [25]. These authors identified the metallic product by XPS.

To study the mechanism of the electrochemical reaction of $CoFe_2O_4$ with lithium, ex situ ^{57}Fe Mössbauer spectra were recorded for samples discharged and charged at several points during the first cycle (Fig. 9). The spectrum recorded for the original sample has been widely reported [26,27]. It shows two sextets, evidencing the Zeeman interaction occurring at the nucleus levels due to the ferrimagnetic character of the crystalline material. The isomer shift values (0.40 and 0.29 mm s^{-1}) correspond to Fe^{3+} in octahedral and tetrahedral sites respectively. The relative contribution of the subspectra (14.4 and 85.6%) is indicative of a partial degree of spinel inversion. For the electrode discharged at 2 F mol^{-1}, the sextets are replaced by three superparamagnetic signals. The loss of crystallinity, usually detected in these electrochemical conversion reactions, induces the formation of smaller domains and thus precluding the ferrimagnetic interaction [11]. A split signal appears at. 1.00 mm s^{-1} that could be assigned to electrochemically reduced Fe^{2+}. Additionally, two signals at 0.37 and 0.32 mm s^{-1} are ascribed to superparamagnetic Fe^{3+} not yet reduced. In a previous work, we described the occurrence of two different locations for iron atoms in the amorphous electrode [11]. The highly split signal is due to iron ions located in more anisotropic sites at the particle surface, while the less split signal was assigned to inner atoms in a more isotropic surrounding. On increasing the charge passed through the cell, Fe^{2+} signal diminishes and eventually disappears at 8 F mol^{-1}. Meanwhile, Fe^{3+} signals evolved distinctly. At 4 F mol^{-1}, we observe a slight reduction of the isomer shift to 0.30 and 0.27 mm s^{-1}, indicating a certain degree of reduction. Otherwise, two significant features can be highlighted in the spectra recorded at 6 F mol^{-1}. First, a notorious increase of the relative contribution of the highly splitted signal was monitored. The continuous loss of crystallinity yields smaller particles in which a large number of iron atoms are located at the particle surface. Moreover, its isomer shift did not decrease and values close to 0.27 mm s^{-1} remained up to 8 F mol^{-1}. In fact, these surface ions are more prone to be oxidised by the contact with the electrolyte precluding an effective electrochemical reduction. Second, the less split signal isomer shift continuously decreased and values close to that of metallic iron (0.11 mm s^{-1}) were recorded for 10 F mol^{-1}.

From these results, a non-homogeneous reduction of iron atoms, affected by their location in the particle, can be inferred. The reduced oxidation state of the inner iron atoms is more efficiently preserved, while those atoms located at the particle surface remain in a higher average valence. Likely, charge trans-

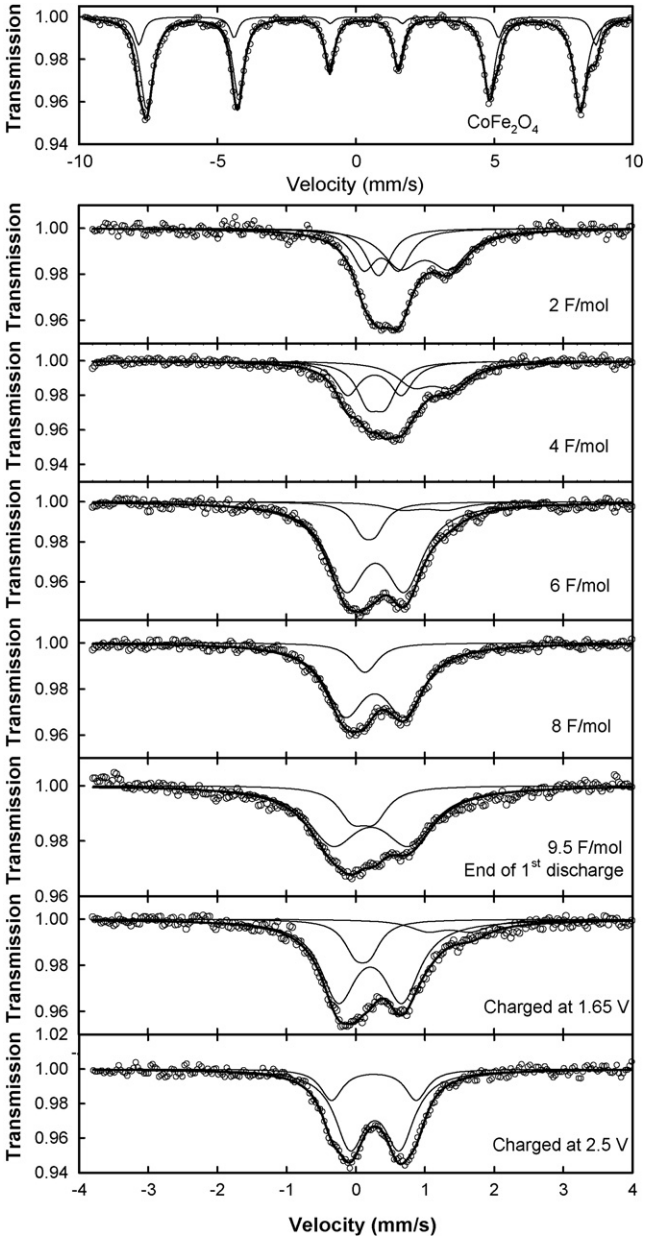

Fig. 9. ^{57}Fe Mössbauer spectra of $CoFe_2O_4$, annealed at 800 °C for 24 h, and partially discharged and charged electrodes. Kinetic rate: 1 C.

fer occurred with the surrounding electrolyte, thus, contributing to the formation of the organic polymer layer.

On charging, the reversibility of the process is evidenced by the iron oxidation. At 1.6 V, the signal attributed to Fe^{2+} is observed again. At 2.5 V, only two superparamagnetic doublets are present. The isomer shift values 0.26 and 0.28 mm s^{-1} involve a partial oxidation ascribable to an average oxidation state rather than the presence of Fe^{3+} or Fe^{2+} separately.

The dramatic changes in particle morphology, at which these samples are submitted upon cycling, are determinant for the elevated polarization detected between charge and discharge branches. For this reason, the study of the kinetic response of the electrode materials was evaluated by cycling lithium test cell at different rates (Fig. 10). The capacity value at the 10th cycle

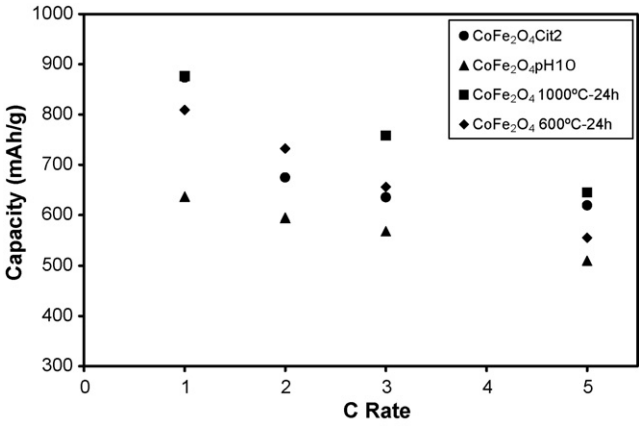

Fig. 10. Plot of capacity versus C rate for $CoFe_2O_4$ prepared by different sol–gel routes.

was plotted against the C rate. $CoFe_2O_4$ samples obtained from a precursor with a 1:2 M:Cit ratio showed an abrupt decrease of capacity at 2 C, though more constant values were recorded by increasing the current to a 5 C rate. A more steady decrease in capacity was detected for $CoFe_2O_4$pH10 sample although lower values of capacity were measured in the whole range. The effect of annealing temperature was evaluated in samples heated at 600 and 1000 °C. A linear decrease was observed in both cases being sharper for the sample heated at 600 °C.

An explanation of this behaviour may arise from the study of the impedance spectra measured on samples cycled at C rate. Fig. 11 displays some Nyquist plots obtained for $CoFe_2O_4$Cit2 and $CoFe_2O_4$pH10. The three electrode test cells were monitored at the end of selected discharges. Two depressed semicircles appear at high and intermediate frequencies. These semicircles are respectively assigned to lithium migration through the electrolyte/inorganic SEI film and charge

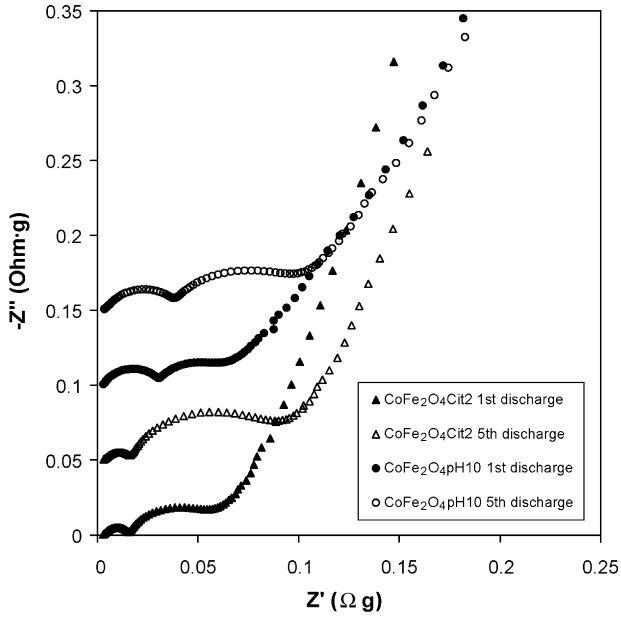

Fig. 11. Nyquist plots for $CoFe_2O_4$Cit2, $CoFe_2O_4$pH10 samples after the first and fifth discharges.

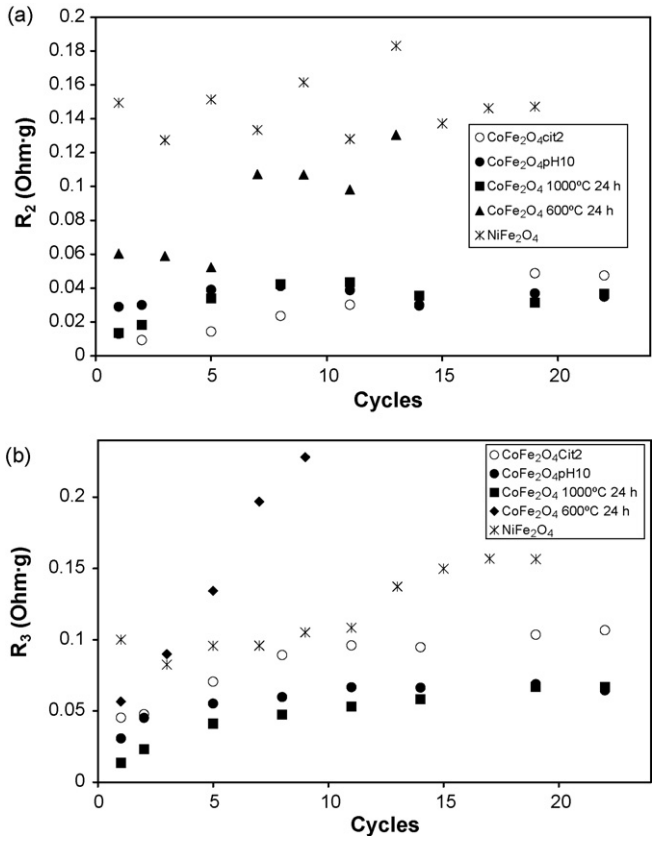

Fig. 12. Variation of (a) SEI (R_2) and (b) charge transfer (R_3) resistance values upon several cycles for $CoFe_2O_4$Cit2, $CoFe_2O_4$pH10, $NiFe_2O_4$ samples annealed at 900 °C for 6 h and $CoFe_2O_4$ at 600 and 1000 °C for 24 h.

transfer through the particle surface [28]. At low frequencies, a huge semicircle is barely revealed. A recent report correlated this last feature to a pseudo-capacitance behaviour, most likely related to the growth of the polymeric organic layer [29]. The variation of the resistance values ascribed to these processes is shown in Fig. 12. R_3 values were higher than R_2 values indicating that the lithium migration through the metallic particle surface imposes a higher energy barrier than the transport through the Li_2O matrix. R_2 values were more dispersed on cycling than R_3 resistance, although the general trend is a steady increase of the values up to the 10th cycle and constancy for subsequent cycling. This result could be related to the capacity fading observed for the first cycles. Otherwise, $CoFe_2O_4$Cit2, whose capacity values were more affected by the increase of the kinetic rate, is also the sample involved in a more notorious increase of charge transfer resistances on cycling. Moreover, the effect of the annealing temperature on samples with a 1:1 ligand to metal ratio is clearly evidenced by high R_2 and R_3 resistance values for the sample annealed at 600 °C. This fact would justify its low electrochemical performance as compare to samples prepared at higher temperatures.

A new set of samples was obtained by substituting Co by Ni in the ferrite stoichiometry. The XRD patterns plotted in Fig. 13 evidence the purity of the phases annealed at 800 and 1000 °C. For the sample heated at 600 °C, a tiny peak at ca. 33° reveals the presence of minor amounts of hematite. The SEM images

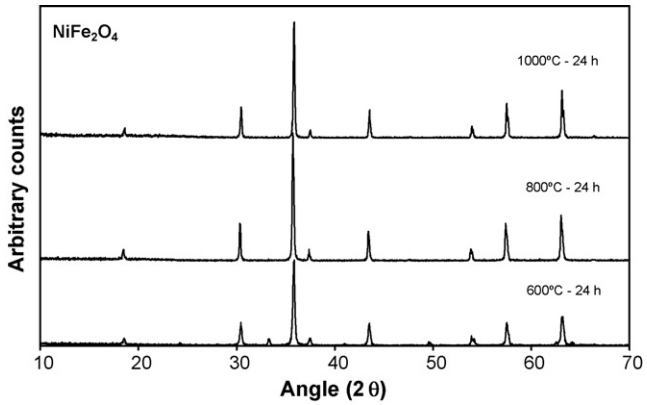

Fig. 13. XRD patterns of $NiFe_2O_4$ annealed at 600, 800 and 1000 °C for 24 h.

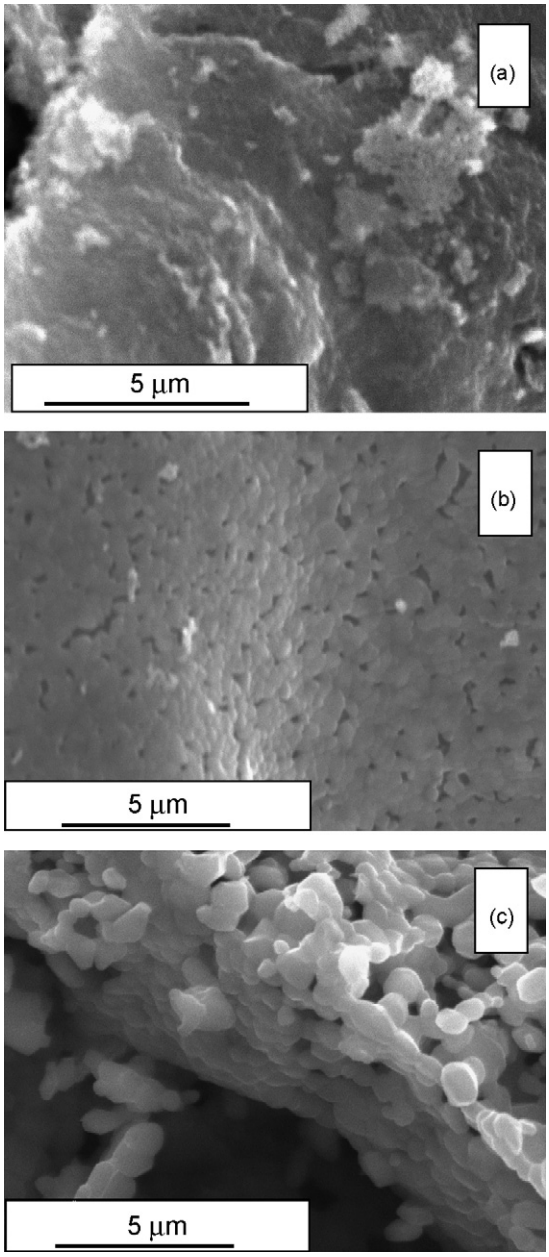

Fig. 14. SEM micrographs of $NiFe_2O_4$ annealed at (a) 600 °C, (b) 800 °C and (c) 1000 °C for 24 h.

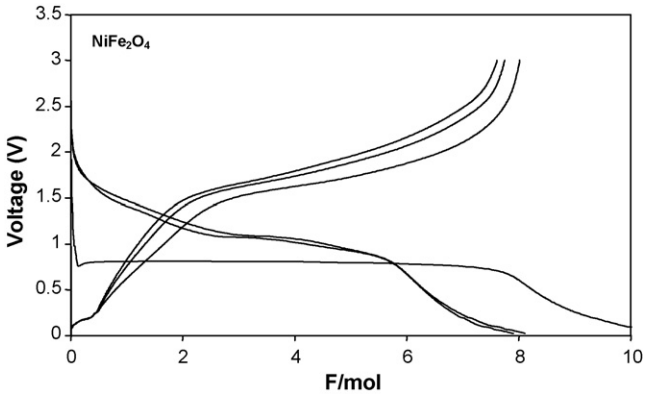

Fig. 15. First galvanostatic curves for $NiFe_2O_4$ annealed at 800 °C for 24 h. Kinetic rate: 1 C.

of the corresponding samples show significant differences as compared to those of $CoFe_2O_4$ prepared in the same conditions (Fig. 14). Less rough surfaces appear in all cases and the increase of temperature involves the occurrence of larger particles closely aggregated precluding the formation of a macroporous system.

The profile of the galvanostatic curves recorded for the first few cycles is quite similar to those previously described for $CoFe_2O_4$. In contrast to that occurring to $NiFe_2O_4$ thin films obtained by PLD method [30], a unique plateau was recorded in the first discharge. This result agrees well with a previous work carried out by our group on $NiFe_2O_4$ obtained by a co-precipitation of an oxalate precursor [11]. The extent of the main reduction plateau in the first discharge matches well with the expected electron consumption for the reduction of the transition metal atoms to their metallic state (Fig. 15). The potential of the discharge plateaus was 0.3 V lower than those of $CoFe_2O_4$. This fact fairly agrees with the less negative Gibb free energy for the NiO formation [31].

The extended cycling of the lithium cells assembled with $NiFe_2O_4$ is plotted in Fig. 15. A capacity fading was recorded in all samples during the first 20 cycles. However, the sample annealed at 800 °C for 24 h was able to maintain capacities higher than 600 mAh g^{-1} after 80 cycles. The lower electrochemical performance of samples annealed at 600 °C and

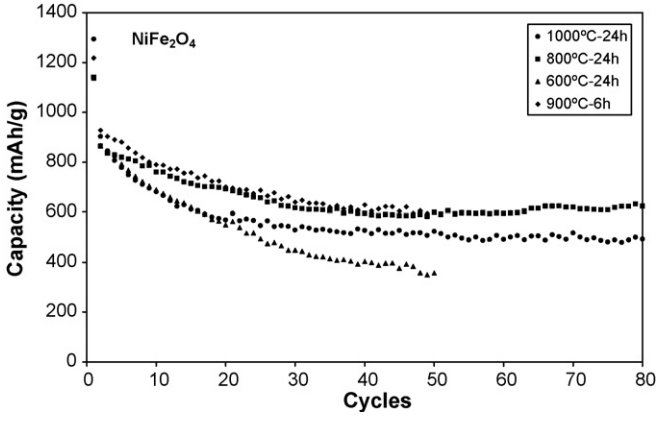

Fig. 16. Galvanostatic cycling of $NiFe_2O_4$ samples annealed at different conditions. Kinetic rate: 1 C.

1000 °C could be ascribable to the shortage of macroporous due to either an uncompleted particle formation or excessive particle aggregation, respectively. The analysis of resistance values measured on the sample annealed at 900 °C for 6 h (Fig. 16) evidences high resistance values in both SEI film (R_2) and charge transfer reaction (R_3) as compared with $CoFe_2O_4$ samples annealed at the same conditions.

4. Conclusions

A sol–gel method based in the precipitation of a metal citrate precursor by a freeze drying procedure has been essayed to obtain $CoFe_2O_4$ and $NiFe_2O_4$. This route of synthesis has demonstrated to be effective for the preparation of pure phases with a tuneable morphology by modifying composition, parameters of the precursor synthesis and annealing conditions. Layered aggregated of primary particles were observed for iron containing samples annealed over 600 °C. This morphology provides a macroporous system which can favours the electrolyte/electrode material contact during the electrochemical process.

Furthermore, the variation of the synthesis conditions introduced in $CoFe_2O_4$ affected significantly to the long-term cycling. Thus, $CoFe_2O_4$ obtained from a precursor with a M:Cit 1:1 ratio, 0.3 M metal concentration and a final pH solution equal to seven demonstrated to be able of sustaining capacities in an extended cycling. The corresponding oxide annealed at 1000 °C for 24 h led to a notorious improvement of the cycling performance. Values as high as 739 mAh g^{-1} were achieved after 75 cycles.

^{57}Mössbauer spectra of partially discharged and charged $CoFe_2O_4$ electrodes evidenced different electrochemical behaviour of core and surface iron atoms. Likely, the high reactivity of electrochemically produced iron atoms favours reactions between the transition metals and the electrolyte avoiding a metallic state at the end of the first discharge.

The kinetic response of the electrode materials was also evaluated by cycling at different rates and impedance spectroscopy of electrodes cycled at C rate demonstrate the sensitivity of $CoFe_2O_4$Cit2 at high rates. It can be related to the high R_2 and R_3 resistance values measured from the Nyquist plots. A slow diffusion of lithium ions through the interfaces clearly affected to the performance of lithium reaction at higher rates.

The freeze-drying process allowed to prepare pure $NiFe_2O_4$. The annealed samples also developed macroporous aggregated whose beneficial effect on the electrochemical reaction is reflected in the ability to maintain capacity values higher than 600 mAh g^{-1} after 80 cycles for the samples obtained at 800 °C for 24 h. The substitution of Co by Ni induced a decrease in the cell voltage of the discharging plateaus, which agrees with the expected changes in the free energy formation of the oxides.

Acknowledgments

We acknowledge financial support from EC (contract SES6-CT2003-503532, ALISTORE), MEC (Contract MAT2005-00374) and Junta de Andalucía (FQM288 group). We also thank to M.C. Mohedano for her technical support and the Central Ser-

vices of the University of Córdoba, and especially to F. Gracia and J. García, for the use of the SEM microscope, FTIR and freeze dryer.

References

[1] P. Poizot, P.S. Laruelle, S. Grugeon, S.L. Dupont, J.-M. Tarascon, Nature (London) 407 (2000) 496.
[2] J.M. Tarascon, S. Grugeon, M. Morcrette, S. Laruelle, P. Rozier, P. Poizot, C.R. Chimie, Electrochem. Commun. 8 (2005) 9.
[3] S. Grugeon, S. Laruelle, L. Dupont, J.-M. Tarascon, Solid State Sci. 5 (2003) 895.
[4] A. Debart, L. Dupont, P. Poizot, J.-B. Leriche, J.M. Tarascon, J. Electrochem. Soc. 148 (2001) A1266.
[5] Y. Liu, K. Horikawa, M. Fujiyosi, N. Imanishi, A. Hirano, Y. Takeda, Electrochim. Acta 49 (2004) 3487.
[6] F. Badway, F. Cosandey, N. Pereira, G.G. Amatucci, J. Electrochem. Soc. 150 (2003) A1318.
[7] Y. Shao-Horn, S. Osmialowski, Q.C. Horn, J. Electrochem. Soc. 149 (2002) A1547.
[8] A. Débart, L. Dupont, R. Patrice, J.-M. Tarascon, Solid State Sci. 8 (2006) 640.
[9] N. Pereira, L. Dupont, J.M. Tarascon, L.C. Klein, G.G. Amatucci, J. Electrochem. Soc. 150 (2003) A1273.
[10] R. Dedryvere, S. Laruelle, S. Grugeon, P. Poizot, D. Gonbeau, J.-M. Tarascon, Chem. Mater. 16 (2004) 1056.
[11] R. Alcántara, M. Jaraba, P. Lavela, J.L. Tirado, J.C. Jumas, J. Olivier-Fourcade, Electrochem. Commun. 5 (2003) 16.
[12] R. Alcántara, M. Jaraba, P. Lavela, J.L. Tirado, Chem. Mater. 14 (2002) 2847–2848.
[13] S. Grugeon, S. Laruelle, R. Herrera-Urbina, L. Dupont, P. Poizot, J.-M. Tarascon, J. Electrochem. Soc. 148 (2001) A285.
[14] D. Larcher, C. Masquelier, D. Bonnin, Y. Chabre, V. Masson, J.-B. Leriche, J.-M. Tarascon, J. Electrochem. Soc. 150 (2003) A133.
[15] M.H. Khedr, A.A. Omar, S.A. Abdel-Moaty, Colloids Surf. A 281 (2006) 8.
[16] F. Bensebaa, F. Zavaliche, P. L'Ecuyer, R.W. Cochrane, T. Veres, J. Colloid Interface Sci. 277 (2004) 104.
[17] Y. Ahn, E.-J. Choi, S. Kim, H.-N. Ok, Mater. Lett. 50 (2001) 47.
[18] D. Larcher, G. Sudant, J.-B. Leriche, Y. Chabre, J.-M. Tarascon, J. Electrochem. Soc. 149 (2002) A234.
[19] R. Alcántara, P. Lavela, J.L. Tirado, E. Zhecheva, R.J. Stoyanova, Solid State Electrochem. 3 (1999) 121.
[20] R. Alcántara, P. Lavela, J.L. Tirado, R. Stoyanova, E. Kuzmanova, E. Zhecheva, Chem. Mater. 9 (1997) 2145.
[21] -Z. Yue, W. Guo, J. Zhou, G. Zhilun, L. Longtu, J. Magn. Magn. Mater. 270 (2004) 216.
[22] C.-H. Lu, H.-H. Chang, -K. Lin, Ceram. Int. 30 (2004) 141.
[23] X. Yang, X. Wang, Z. Zhang, J. Cryst. Growth 277 (2005) 467.
[24] M. Mouallem-Bahout, S. Bertrand, O.J. Peña, Solid State Chem. 178 (2005) 1080.
[25] Y.-Q. Chu, Z.-W. Fu, Q.-Z. Qin, Electrochim. Acta 49 (2004) 4915.
[26] S.-J. Kim, S.-W. Lee, S.-Y. An, C.-S. Kim, J. Magn. Magn. Mater. 215-216 (2000) 227.
[27] T.A.S. Ferreira, J.C. Waerenborgh, M.H.R.M. Mendonça, M.R. Nunes, F.M. Costa, Solid State Sci. 5 (2003) 383.
[28] M. Dolle, Ph. Poizot, L. Dupont, J.-M. Tarascon, Electrochem. Solid-State Lett. 5 (2002) A18.
[29] S. Laruelle, S. Grugeon, P. Poizot, M. Dollé, L. Dupont, J.-M. Tarascon, J. Electrochem. Soc. 149 (2002) A627.
[30] Y.-N. NuLi, Q.-Z. Qin, J. Power Sources 142 (2005) 292.
[31] P. Poizot, S. Laruelle, S. Grugeon, J.-M. Tarascon, J. Electrochem. Soc. 149 (2002) A1212.